



# Microstructure and photocatalytic properties of bismuth oxide ( $\text{Bi}_2\text{O}_3$ ) nanocrystallites

R. Senthamilselvi<sup>1</sup>, R. Velavan<sup>2</sup>

## Abstract

In this work,  $\text{Bi}_2\text{O}_3$  nanoparticles were prepared using the co-precipitation process. The Pentahydrate of Bismuth Nitrate, KOH and Dil. nitric acid was used for the synthesis of the  $\text{Bi}_2\text{O}_3$  nanoparticles. The precipitated liquid was allowed to stir for 2 hours in a water bath at  $60^\circ\text{C}$ , then washed with DI water and dried in an oven at  $80^\circ\text{C}$  for 6 hours, and then calcinated at  $500^\circ\text{C}$ . X-ray diffraction (XRD), Fourier transform infrared (FTIR) spectroscopy, and field emission scanning electron microscopy (FESEM), photoluminescence (PL) and photocatalytic studies have characterized the synthesized  $\text{Bi}_2\text{O}_3$  nanomaterials. The XRD results showed that  $\text{Bi}_2\text{O}_3$  nanoparticles with a monoclinic structure. The FESEM studies showed that  $\text{Bi}_2\text{O}_3$  crystallites were formed with a rod-like structure. The  $\text{Bi}_2\text{O}_3$  nanoparticles are structure-like and agglomerated surfaces. The nanoparticles (1g / l) are applied to the 50 ml of MB dye solution and stored under visible light in the photoreactor to study dye degradation. Studies have shown that  $\text{Bi}_2\text{O}_3$  nanoparticles effectively degrade the MB dye with visible light irradiation. After 150 min of irradiation, the photocatalytic studies showed 71 percent degradation efficiency

## Keywords

Bismuth Nitrate, spectroscopy, photoreactor.

<sup>1,2</sup>Department of Physics, Bharath Institute of Higher Education and Research, Chennai-600073, Tamil Nadu, India.

Article History: Received 01 October 2020; Accepted 10 December 2020

©2020 MJM.

## Contents

1	Introduction.....	4870
2	Materials and methods.....	4871
3	Conclusion.....	4873
	References.....	4873

## 1. Introduction

In recent years, nanomaterials attracted huge interest because of its mechanical properties like high strength to weight ratio (e.g. Carbon Nano Tubes), higher dampening property because of its larger surface to volume ratio and its thermal conductivity. Due to the high surface area of the Metal oxide nanoparticles, applications like sensors, catalysts etc. are studied intensively. One of the major applications of  $\text{Bi}_2\text{O}_3$  nanoparticles is that it's a p-type semiconductor, and its application as a better solid-state electrolyte compared to stabilize Zirconia as the FCC structure of  $\text{Bi}_2\text{O}_3$  provides better ion conductivity compared to other oxide ion conductors [1-4]. Because of the excellent photocatalytic property at visible light range and a proven anti-bacterial, its application in medical field too is enormous [5].

$\text{Bi}_2\text{O}_3$  is a yellow powder. It exists in five crystallographic polymorphs,

1.  $\alpha$ - $\text{Bi}_2\text{O}_3$  (monoclinic)
2.  $\beta$ - $\text{Bi}_2\text{O}_3$  (tetragonal)
3.  $\gamma$ - $\text{Bi}_2\text{O}_3$  (body-centered cubic)
4.  $\delta$ - $\text{Bi}_2\text{O}_3$  (cubic)
5.  $\epsilon$ - $\text{Bi}_2\text{O}_3$  (triclinic)

$\alpha$  and  $\beta$  forms are stable at room and high temperatures, respectively, whereas the other forms are metastable [6]. Bismuth oxide nanoparticles made using  $\text{Bi}(\text{NO}_3)_3 \cdot 6\text{H}_2\text{O}$  as precursor are used in a processes including precipitation [7], hydrothermal/solvothermal method [8, 5], sol-gel methods [9], and flame spray pyrolysis [10]. While basic spherical nanoparticles are more popular [5],  $\text{Bi}_2\text{O}_3$  nanowires [11], nanofibers [12] and nanoflakes [13] are also used.

### Applications of $\text{Bi}_2\text{O}_3$ particles

1. Used in Solid-oxide fuel cells (SOFCs) as solid electrolyte.

- Bismuth Oxide Nanoparticles in Drug Delivery Systems because of its visible light photocatalytic properties.
- Have photocatalytic anti-bacterial properties towards E-coli bacteria.
- Removal of heavy metal Chromium VI in water purification process.

**Table 1: Structural and Physical Properties of  $\text{Bi}_2\text{O}_3$** 

1	Chemical formula	$\text{Bi}_2\text{O}_3$
2	Molar mass	465.96 g/mol
3	Structure	Monoclinic crystal
4	Lattice constant	structure ( $\alpha\text{-Bi}_2\text{O}_3$ )
5	Appearance	$a = 5.589\text{\AA}$
6	Density	Yellow powder
7	Melting point	$8.86\text{ g/cm}^3$
8	Boiling point	$817^\circ\text{C}$
9	Band gap Magnetic	$1890^\circ\text{C}$
10	susceptibility ( $\chi$ ) Re-	$2.91\text{ eV } (\alpha\text{-Bi}_2\text{O}_3)$
11	fractive index	$-83.0 \times 10^{-6}\text{ cm}^3/\text{mol}$
		2.5

## 2. Materials and methods

### 2.1 Materials

The materials such as Bismuth nitrate pentahydrate, KOH and dil. Nitric acid DI water are used in the synthesis of Bismuth oxide material. The precursor materials are of AR grade and are used directly for the synthesis.

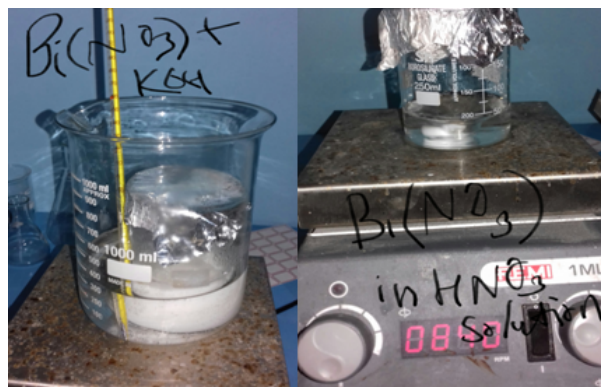
Conc. Nitric acid was diluted in 50 ml of DI water and stirred for about 10 minutes. Bismuth nitrate pentahydrate was dissolved in dil. nitric acid solution and allowed to stir for 30 minutes. 5.610g of KOH pellets was dissolved in 40 ml of DI water and KOH solution was added in drops to the precursor solution. The final precipitated liquid was allowed to stir at  $60^\circ\text{C}$  in a water bath for 2 hours. Wash the sample with distilled water (Note: pH has to be maintained above 12). Dry it at  $80^\circ\text{C}$  for 6 hours in an oven and then calcinated the sample at  $500^\circ\text{C}$  for 2 hours.

### 2.2 Synthesis of $\text{Bi}_2\text{O}_3$ using Co-precipitation method

In this technique, the size of the materials can mainly be controlled. The synthesis involves reaction in a suitable solvent between critical materials. Until precipitation reaction, the dopant will be added to the precursor solution. Surfactant is used to preserve the separation between the formed particles [14].

During this process, the metal cations are precipitated as hydroxides, oxalates, carbonates or citrates. The final powder product (nanomaterial) is obtained by calcinations of the precipitate at suitable temperatures. Regarding precipitation technique, the required calcinations temperature for the formation of the nanoparticles is low due to its atomic scale mixing. As the calcination temperature is low, the energy consumption is observed to be low with less pollution. The low temperature calcinations will result in lower particle size.

Depending on the concentration of precursor solution, stirring speed, temperature and pH value, the properties of the obtained nanoparticles will vary. For a desired property, one needs to vary these parameters.


**Figure 1. Synthesis of Bismuth Oxide ( $\text{Bi}_2\text{O}_3$ )**

Moreover, co-precipitation reactions reveal the following characteristics features. Under the highly super saturated state, the chemical reaction will induce precipitation and the obtained product will be insoluble in nature. Nucleation is an important step, and the particles formation will be large in numbers. Secondary processes like aggregation of the particles and Ostwald ripening will considerably affect the grain size, morphology, and properties. The precursors involved in this process are cheaper in market and the process is the most economical route. The final product is highly pure with well-defined and controlled size of nanoparticles, nanorods and nanotubes.

### 2.3 Characterization Techniques

X-ray diffractometer with CuK $\alpha$  radiation ( $1.5418\text{ \AA}$ ) (Rigaku, Japan) is used to analyze the structure of the sample. The sample is scanned for a  $2\theta$  ( $20 - 90^\circ$ ) range with a phase size of  $0.02^\circ$ . For chemical analysis, the FTIR spectrometer, (Spectrum Two FTIR / ATR spectrometer) in the wavenumber range of  $400\text{-}4000\text{ cm}^{-1}$  with a resolution of  $0.5\text{ cm}^{-1}$ , is used to confirm the chemical bonds in the sample. The sample was absorbed using a double beam spectrophotometer (UV-1800, Shimadzu) with a wavelength range of  $200\text{-}1000\text{ nm}$ .  $1\text{ nm}$  is the resolution. To find the bandgap and defects in the sample, a photoluminescence setup (Model: LS 45 Spectrofluorometer) of  $350\text{ nm}$  excitation wavelength and a resolution of  $1\text{ nm}$  is used. The sample is non-conducting in the current analysis, which is why a very thin gold layer of around  $10\text{ nm}$  is sputter-coated for conduction. A field emission scanning electron microscope (FESEM) (Carl Zeiss microscopy ltd, UK & SIGMA) was used to analyse the morphology and composition. Advanced analytical microscopy is provided by Field Emission Scanning Electron Microscopes (FE-SEM). With its in-lens secondary electron detection, the GEMINI column provides you with unprecedented resolution, contrast and brightness for highly topographical imaging samples. With a high vacuum mode of operation, performing and non-conducting samples are defined as images. With an acceleration voltage of  $0.2\text{-}30\text{ kV}$ , the FESEM magnifi-



cation is 10-1,000,000 X. Structures as small as 1.5 nm are resolved. Bismuth oxide nanoparticles are used as catalyst and its photocatalytic performance is studied using the photoreactor (HEBER, MODELHVAR-MP400) with visible light and 300 Watts. The degradation was carried out for 2 hrs after the dark condition.

## Results & discussion

### X-ray diffraction (xrd) analysis

Fig. 2 reveals the XRD pattern of  $\text{Bi}_2\text{O}_3$  NPs with microrod-like structures. Due to four polymer types ( $\alpha$ - $\delta$ - $\text{Bi}_2\text{O}_3$ ,  $\beta$ - $\delta$ - $\text{Bi}_2\text{O}_3$ ,  $\gamma$ - $\delta$ - $\text{Bi}_2\text{O}_3$ , and  $\delta$ - $\text{Bi}_2\text{O}_3$ ),  $\text{Bi}_2\text{O}_3$  has distinct crystalline structures and properties. The sample's crystalline stage is defined by the XRD pattern. According to the normal diffraction spectrum of  $\alpha$ - $\text{Bi}_2\text{O}_3$ , the XRD pattern reveals the crystalline  $\text{Bi}_2\text{O}_3$ . In compliance with JCPDS No. 41-1449, all peaks are indexed. The oxide observed belongs to  $\alpha$ - $\text{Bi}_2\text{O}_3$ , which crystallises in the structure of the monoclinic. This finding is consistent with the other recorded results[15-18], which address the different allotropics obtained on the basis of the temperature range used for bismuth oxide synthesis. Scherrer formula crystallite size estimate applied to the peak (120) and found to be 54 nm.

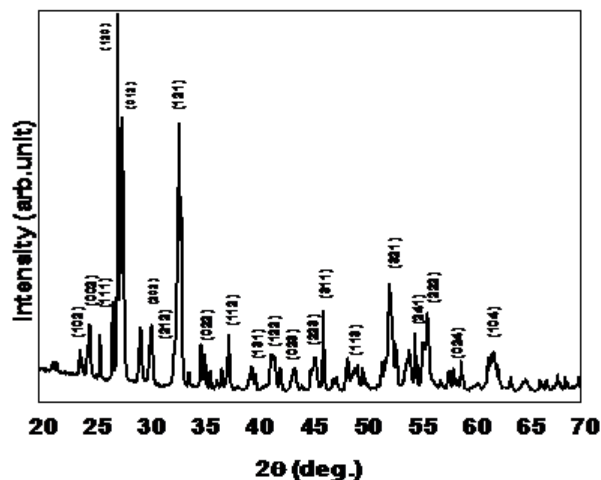


Figure 2. XRD pattern of  $\text{Bi}_2\text{O}_3$  nanoparticles

Fig. 3 displays the Bismuth oxide sample's FTIR spectrum. The spectrum displays ~ 3460 absorption lines. 2982, 2870, 2660, 2080, 1470, 1385, 826, 575 and 520  $\text{cm}^{-1}$ , respectively. O-H vibration, suggesting the presence of the water molecule and the hydroxyl group, is attributed to a band at 3460  $\text{cm}^{-1}$ . The 575 and 520  $\text{cm}^{-1}$  bands are the Bi-O-Bi bond's stretching vibrations. Y. Zhang et al showed that the bands at 605 and 534  $\text{cm}^{-1}$  are the Bi-O band's stretching vibrations and the metal-oxygen bonds are due to a weak peak close to 553  $\text{cm}^{-1}$  [18]. The peaks at 3300-3500  $\text{cm}^{-1}$  are the stretching vibration that is produced during the synthesis phase of the absorbed hydroxyl function groups.

The surface topography of the prepared  $\text{Bi}_2\text{O}_3$  was studied using FE-SEM. The FESEM images of the sample (Fig. 4), revealed pure crystalline  $\text{Bi}_2\text{O}_3$  with highly compact plate like

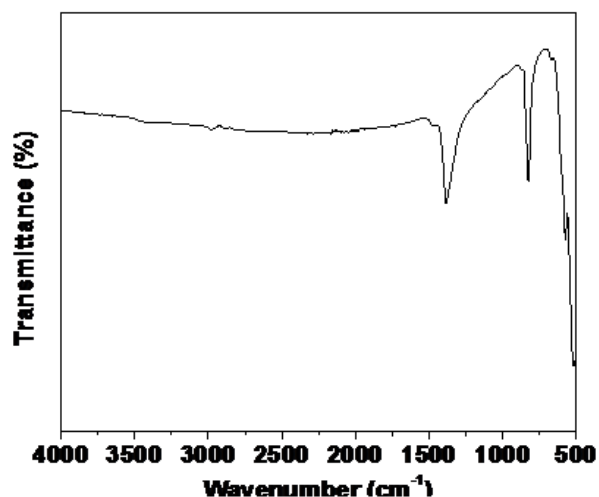


Figure 3. FT-IR spectrum of  $\text{Bi}_2\text{O}_3$  nanoparticles

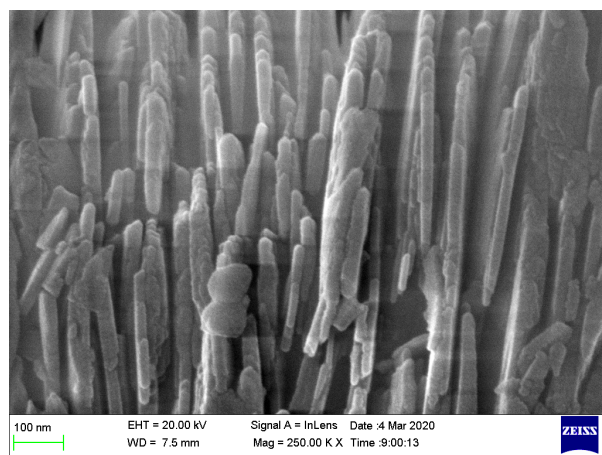


Figure 4. FE-SEM images of  $\text{Bi}_2\text{O}_3$  nanoparticles

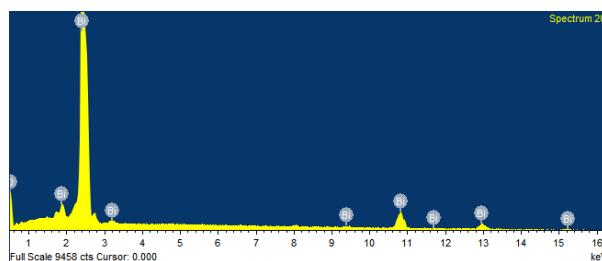


Figure 5. EDAX spectrum of  $\text{Bi}_2\text{O}_3$  nanoparticles

structure. High resolution images revealed the  $\text{Bi}_2\text{O}_3$  exists as individual nanorod like structure with dense structure [19].

### Photocatalytic studies

The degradation rate of MB dye solution in a photochemical reactor assesses the photocatalytic efficiency of samples. As a visible light source, it is fitted with a 300 W lamp, which is about 10 cm from the liquid surface of the suspension. Samples of 50 mg are applied under continuous magnetic stirring in a 50 mL MB dye solution (1g / l). In the dark state, the dye solution is stirred for 30 minutes before illumination to



achieve the equilibrium of adsorption-desorption. At a pace of 5000 rpm / min, 3 mL suspensions are removed and centrifuged in a timely manner for 5.0 min. The UV-Visible spectrophotometer tests the absorbance of the supernatant at 665 nm. The rate of deterioration (percent) is determined according to the formula below:

$$W = (1 - A_t / A_o) \text{ about } 100\%$$

Where  $A_o$  and  $A_t$  are the absorption of MB dye solution before lighting and after illumination at the time of  $t$ .

Fig. 6 indicates MB degradation as a result of the time of irradiation under visible light over the catalyst. It is noted that the deterioration is obviously time-related. The resulting efficiency of degradation is almost 71 percent after 150 minutes of visible light irradiation.

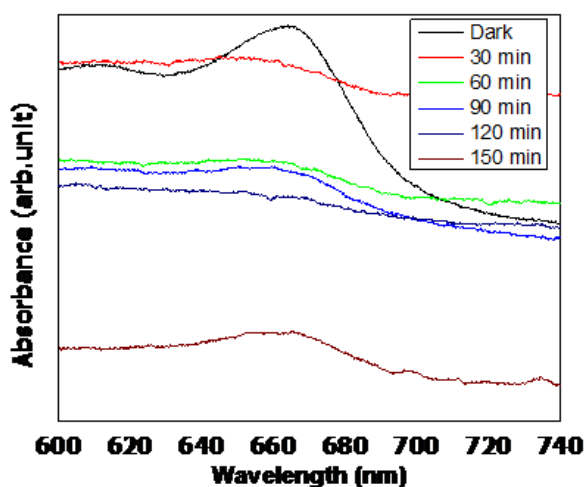


**Figure 6.** Photocatalytic studies of  $\text{Bi}_2\text{O}_3$  nanoparticles with MB dye under visible light

Using the solid state reaction process, Hicham Oudghiri-Hassani et. al., synthesised  $\text{Bi}_2\text{O}_3$  bismuth oxide nanoparticles. The monoclinic structure of  $\text{Bi}_2\text{O}_3$  at 280 °C was suggested. As confirmed by the Scherrer formula, the crystallite size of the particles was 150 nm. These particles are used to degrade rhodamine B, a pollutant under UV radiation, as a catalyst [15]. The pure bismuth oxide NPs were prepared by Iyyapushpam et al at room temperature using a chemical process. The formation of  $\text{Bi}_2\text{O}_3$  was confirmed by XRD. SEM is used to observe the morphology of the NPs. Photocatalytic studies of  $\text{Bi}_2\text{O}_3$  are carried out by 2h aqueous solution decolorization with MB dye. The efficiency of degradation of  $\text{Bi}_2\text{O}_3$  depends on the size of the crystallite. For as-prepared and annealed, the degradation percentage of MeO is 76 percent, 52 percent and 24 percent for the samples annealed at 200 and 600 °C, respectively [19]. Pure and doped  $\text{Bi}_2\text{O}_3$  nanoparticles were synthesised by Raza et al through the sol gel process. Monoclinic  $\alpha\text{-Bi}_2\text{O}_3$  revealed the XRD pattern of the  $\text{Bi}_2\text{O}_3$  nanoparticles. The photocatalytic performance of the photocatalyst was analysed as a result of the time of irradiation by the degradation of different dyes [20,21].

### 3. Conclusion

In summary, by a simple and successful co-precipitation process,  $\text{Bi}_2\text{O}_3$  nanopowders with microrod-like structures were obtained. XRD, FTIR, FESEM, and photoreactor are analysed in the synthesized bismuth oxide sample to study its microstructure and photocatalytic properties. The XRD pattern showed that the monoclinic structure of well crystalline  $\text{Bi}_2\text{O}_3$  was established. The FESEM picture clearly shows the vertically arranged, crystalline-like morphology of the rod. The prepared  $\text{Bi}_2\text{O}_3$  NPs are used for the degradation of MB dye using visible light irradiation as a photocatalyst. The sample demonstrated strong photocatalytic behaviour under visible light and displayed degradation efficiency. It is concluded that synthesized nanoparticles can be used to degrade contaminants as a catalyst.

### References

- [1] P. Suk, H.D. Wiemhofer, U. Guth, W. Gopel, M. Greenblatt, *Solid State Ionics*, 89 (1996) 179.
- [2] M. Matsuoka, *Jpn. J. Soc. Appl. Phys.*, 10 (1971) 736.
- [3] G.S. Devi, S.V. Manorama, V.J. Rao, *Sens. Actuators*, B 56 (1999) 98.
- [4] L. Moens, P. Ruiz, B. Delmon, M. Devillers, *Catal. Lett.*, 46 (1997) 93.
- [5] F. Qin, H. Zhao, G. Li, et al., *Nanoscale*, 6 (2014) 5402–5409.
- [6] M. K. Trivedi, R. M. Tallapragada, A. Branton, et al., *Am. J. Nano Res. Appl.*, 3(6) (2015) 94–98.
- [7] S. A. Hosseini and R. Saedi, *Bull. Chem. React. Eng. Catal.*, 12(1) (2017) 96 – 105.
- [8] K. K. Bera, R. Majumdar, M. Chakraborty, et al., *J. Hazard. Mater.*, 352 (2018) 182–191.
- [9] M. Mallahi, A. Shokuhfar, M. R. Vaezi, et al, *AJER*, 3(4) (2014) 162–165.
- [10] T. Rudin, K. Wegner and S. E. Pratsinis, *J. Nanopart. Res.*, 13(7) (2011) 2715 – 2725.
- [11] S. Park, S. An, H. Ko, et al., *J. Nanosci. Nanotechnol.*, 15(2) (2015) 1605 – 1609.
- [12] K. Brezesinski, R. Ostermann, P. Hartmann, et al., *Chem. Mater.*, 22(10) (2010) 3079 – 3085.
- [13] J. Wang, X. Yang, K. Zhao, et al., *J. Mater. Chem.*, A 1(32) (2013) 9069 – 9074.
- [14] G. D'Costa, DS Pisal, AV Rane; Report on Synthesis of nanoparticles and functionalization: Co precipitation method, (2012).
- [15] Hicham Oudghiri-Hassani, Souad Rakass, Fahd T. Al Wadaania, Khalaf J. Al-ghamdia, Ahmed Omera, Mouslim Messalia, Mostafa Abboudia, *Journal of Taibah University for Science*, (2015).
- [16] Xiaoni Du & Yang Liu & Xiaohong Wang & Jingqing Feng & Chaofei Ren, *Journal of the Australian Ceramic Society*, (2018).
- [17] Xiaogang Guo, TaoTao Liang, Matthew Rager, Xun Cui, (2018).



- [18] S. Iyyapushpam, S.T. Nishanthi, D. Pathinettam Padiyan, *Materials Letters*, 86 (2012) 25–27.
- [19] Yu Zhang, Qian Shao, Chunyu Chen, Heyun Jiang, Fengmei Su, Qian Hu, Zhanhu Guo, *Powder Technology*, (2019)
- [20] Waseem. Raza, M.M. Haque, M. Muneer, T. Harada, M. Matsumura, *Journal of Alloys and Compounds*, (2015).

\*\*\*\*\*  
ISSN(P):2319 – 3786  
Malaya Journal of Matematik  
ISSN(O):2321 – 5666  
\*\*\*\*\*

